Redox behavior of yttrium and electrochemical formation of Y-Al alloys in molten chlorides

He, Jiwen; Hua, Zhongsheng; Liu, Huan; Xu, Liang; He, Shiwei; Yang, Yongxiang; Zhao, Zhuo

DOI
10.1149/2.1231811jes

Publication date
2018

Document Version
Final published version

Published in
Journal of the Electrochemical Society

Redox Behavior of Yttrium and Electrochemical Formation of Y-Al Alloys in Molten Chlorides

Journal of The Electrochemical Society, **165** (11) E598-E603 (2018)
0013-4651/2018/165(11)/E598/6/$37.00 © The Electrochemical Society

Redox Behavior of Yttrium and Electrochemical Formation of Y-Al Alloys in Molten Chlorides

Jiwen He,[1] Zhongsheng Hua,[1,z] Huan Liu,[1] Liang Xu,[1] Shiwei He,[1] Yongxiang Yang,[1,2] and Zhuo Zhao[1,z]

[1] *School of Metallurgical Engineering, Anhui University of Technology, Ma'anshan 243032, People's Republic of China*
[2] *Department of Materials Science and Engineering, Delft University of Technology, 2628 CD Delft, The Netherlands*

The electrochemical behavior of yttrium and its co-deposition with aluminum were investigated by several transient electrochemical techniques on a tungsten electrode at 973K in NaCl-KCl eutectic melts. The results reveal that the reduction of Y(III) in NaCl-KCl-YCl_3 melts is a one-step process with three-electron exchanged and the reaction is a quasi-reversible diffusion-controlled process at low scan rates (0.05∼0.5 V/s). The calculated diffusion coefficient is approximately $2.8 \times 10^{-5}cm^2/s$. After $AlCl_3$ was introduced into the melts, cyclic voltammetry and open circuit chronopotentiometry showed the formation of two Y-Al intermetallic compounds, indicating that under-potential deposition of yttrium occurred on tungsten electrode covered with liquid Al. The electromotive force was measured at 973K to determine the thermodynamic properties of Y-Al intermetallic compounds, such as the activity of Y in the two-phase coexistence state, relative partial molar Gibbs energies, as well as the standard Gibbs energies of Y-Al intermetallic compounds. Finally, potentiostatic electrolysis was conducted to prepare Y-Al alloys from molten NaCl-KCl-YCl_3 (1.5 mol%)-$AlCl_3$ (1.5 mol%) by the co-reduction method. The cathodic alloys were characterized using X-ray diffraction (XRD) and scan electron micrograph (SEM)-energy dispersive spectrometry (EDS) and the results indicated that the obtained alloys were mainly composed of YAl_2, as well as YAl_3 and YAl phases. The Y-rich phase intermetallic compound YAl, formed in the later period of electrolysis just when the concentration of $AlCl_3$ is fairly low.
 [DOI: 10.1149/2.1231811jes]

Manuscript submitted July 17, 2018; revised manuscript received August 15, 2018. Published September 7, 2018.

Nowadays, rare earth (RE) elements, the so-called critical raw materials, are playing a crucial role in the field of advanced materials, such as hydrogen storage alloys, high-performance magnets, fluorescent materials, optical glass, etc.[1] Among them, RE elements are usually used in the form of their alloys. It was found that the addition of RE element can optimize the microstructure and improve the corrosion resistance and mechanical properties of most alloys.[2–4] These important applications are expected to increase the demand for rare earth metals and their alloys in the future.[5]

Y-Al alloys are widely used in automotive, aerospace and aviation industry,[6,7] and more importantly, they are also excellent hydrogen storage materials[8] due to the considerably low density and high tensile strength.[9] With their increasing applications in other fields and transition to a green economy, the demand for Y-Al alloys will continue to increase in the near future. Currently, most RE-Al alloy is prepared via directly mixing and melting pure Al with RE metals in industry. This conventional method has several disadvantages including serious metal oxidation, inhomogeneous alloy composition and high energy consumption. Molten salt electrolysis is an effective method for alloy production owing to its advantages of simple process, low cost, and high efficiency.[10] In particular, the composition of the alloys can be adjusted by controlling the electrochemical parameters.[11]

There have been a number of reports on the preparation of RE-Al alloys by molten salt electrolysis. Castrillejo et al.[12] obtained the Dy–Al alloys in the LiCl–KCl–$DyCl_3$ system using an Al cathode at 723K. Su et al.[13] prepared Dy–Al alloys on the tungsten electrode by electrolyzing in LiCl-KCl-$AlCl_3$-Dy_2O_3 melts at 773K, however only a very small amount of products was produced due to the small cathode current and the high melting point of the alloys. Afterwards, they chose Al cathode instead of the tungsten electrode during electrolysis in LiCl-KCl-$AlCl_3$ (1.2wt%)-Dy_2O_3 (0.9wt%) melts, and thus single Al_3Dy intermetallic compound was obtained through potentiostatic electrolysis at −1.5 V and −1.6 V while two intermetallic compounds $DyAl_3$ and DyAl were gained by galvanostatic electrolysis at −50 mA. Bermejo et al.[14] also used Al as the cathode and obtained Al_3Lu by adding $LuCl_3$ into the LiCl–KCl eutectic through potentiostatic electrolysis at 773K. Yan et al.[15] prepared various Al-Li-Eu intermetallics in the LiCl-KCl-$AlCl_3$-Eu_2O_3 melts at 773 K by controlling the amount of $AlCl_3$ in the system. Li et al.[16] directly prepared Mg-Li-Al-Yb alloys in the LiCl-KCl-$MgCl_2$-$AlCl_3$-Yb_2O_3 melts at 923 K, and the corrosion resistance of the alloys was investigated by potentiodynamic polarization in 3.5 wt% NaCl. They found that Al_2Yb is a stable phase in Mg-Li-Al-Yb alloys.

Moreover, there have been some studies on the electrochemical behavior of yttrium in different systems and the preparations of Y-Al based alloys. Li et al.[17] prepared Mg-Al-Y alloys on a molybdenum electrode in the molten LiCl-NaCl-$MgCl_2$-AlF_3-YCl_3 salts. They found that the concentration of YCl_3 has a great influence on alloy composition and the existence of Y in the alloys can inhibit the formation of Mg-Al compound. Li et al.[18] investigated the electrochemical behavior of yttrium on the Mo and Al electrodes in LiCl-KCl-$AlCl_3$-Y_2O_3 system. Al-Li-Y alloys with different Y contents were obtained on the Mo electrode by galvanostatic electrolysis, and lithium and yttrium contents in the alloys depended on the concentration of $AlCl_3$ in the melts. However, the electrochemical signals of Y-Al intermetallic compounds were ignored in this work. Yan et al.[19] successfully prepared Al-Y alloys composed of Al_2Y and α-Al_3Y in LiCl-KCl-$AlCl_3$-Y_2O_3 melts, and revealed the electrochemical formation of these two intermetallic compounds clearly. Nevertheless, the electrochemical behavior of Y(III) and its co-reduction with Al(III) in molten NaCl-KCl eutectic have not been reported in the current literatures. In present work, the electrochemical co-reduction behavior of Y(III) and Al(III) ions in NaCl-KCl molten salts was systematically investigated by employing cyclic voltammetry and open circuit chronopotentiometry, and then the thermodynamic properties of different Y-Al intermetallic compounds were determined at temperatures of 973K by electromotive force measurements. Finally, Y-Al alloys were fabricated by potentiostatic electrolysis in the NaCl-KCl-YCl_3-$AlCl_3$ system at 973K, and characterized by XRD and SEM-EDS.

Experimental

Preparation and purification of electrolyte.—The mixture of eutectic salts (NaCl:KCl = 50.6:49.4 mol%) was chosen as the supporting electrolyte due to its high theoretical decomposition voltage and low eutectic point, the natural abundance of sodium and potassium. Firstly, analytical reagents of NaCl (>99.5% AR grade) and KCl (>99.5% AR grade) were dried at 473K for 72 hours in vacuum to remove excess water, and then pre-electrolysis was performed at −2.10 V for 3 h in an alumina crucible (99.5 wt% Al_2O_3) in an electric furnace for the removal of other metal ions impurities in the melts. Y(III) and Al(III) cations were added into the melts in the form

[z]E-mail: huazs83@163.com; zhaozhuo1018@163.com

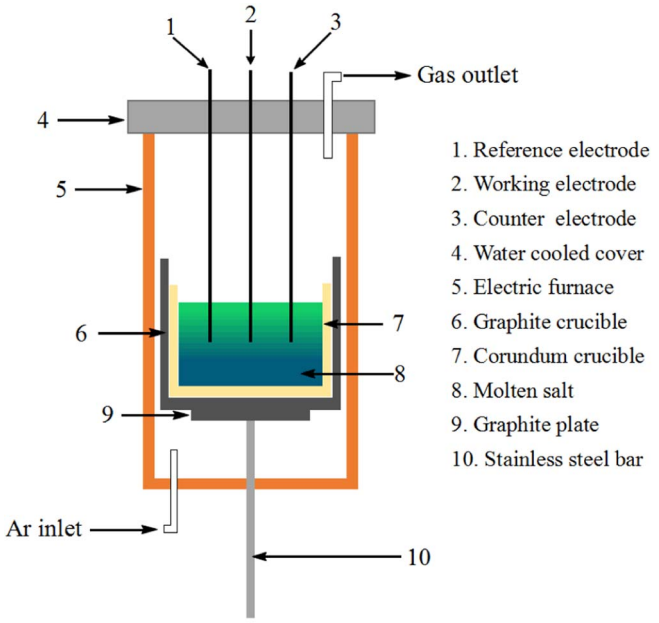

Figure 1. Schematic diagram of the electrochemical experimental device.

of anhydrous YCl_3 (99.99%) and $AlCl_3$ (99.6%), respectively. All experiments were performed with high purity argon protection.

Electrochemical apparatus and electrodes.—All the electrochemical experiments were performed using the PARSTAT 2273 electrochemical workstation (Ametek Group Co, American) with the PowerSuite software package. Three-electrode cell was used in all the electrochemical measurements, as shown in Fig. 1. A tungsten wire (99.99% purity, 1.0 mm in diameter) was employed as the working electrode. A spectral pure graphite rod (6.0 mm in diameter) served as the counter electrode. A silver wire (99.99% purity, 1.0 mm in diameter) immersed in a solution of NaCl-KCl-AgCl (1 wt%) contained in a mullite tube was adopted as the reference electrode. All potentials were referred to this Ag^+/Ag couple in this study. The surface area of the working electrode was calculated after each experiment by measuring the immersion depth of the electrode in the melts.

Potentiostatic electrolysis and characterization of cathode deposits.—The Y-Al alloys were prepared by potentiostatic electrolysis on a tungsten electrode at 973K. After electrolysis, all the cathodic products were initially immersed in distilled water to remove the residual salts and then ultrasonically cleaned with ethanol (99.5%). The phase composition of the samples was analyzed by XRD (D8 Advance, Bruker axs) using a Cu Kα monochrome target. Microstructures were examined using SEM (SSX-550, Shinadzu Corporation), and microanalysis was performed simultaneously using energy dispersive X-ray spectroscopy (EDS) with SEM.

Results and Discussion

Electrochemical behavior of yttrium.—Fig. 2 shows the cyclic voltammograms measured on tungsten electrodes before and after the addition of YCl_3 in the NaCl-KCl system at 973K. The dashed line in Fig. 2 represents the cyclic voltammogram of the purified blank salts. The cathodic peak A_2 appearing at −2.20 V (vs Ag/AgCl) is ascribed to the deposition of Na, and its corresponding anodic peak A_1 in the reverse scan direction is attributed to the dissolution of metallic Na. Except for the redox peaks A_1/A_2, there are no additional reaction signals in the electrochemical window, indicating that the NaCl-KCl melts were suitable for our investigations. The solid line shows the cyclic voltammogram after the addition of YCl_3 in the

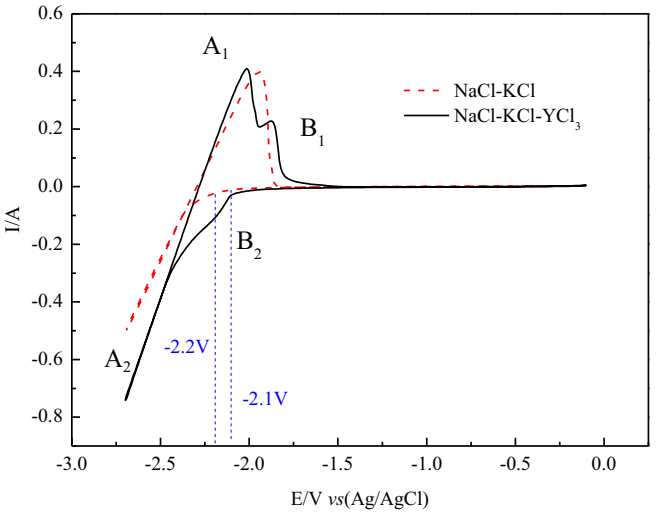

Figure 2. Cyclic voltammograms measured on a tungsten electrode (d = 1 mm) before and after addition of 0.6 mol% YCl_3 in NaCl-KCl system at 973 K, scan rate = 0.1 V/s.

molten salts. A new pair of redox peaks B_2/B_1 appear in the range of −2.10∼−1.96 V, which are considered to be the deposition of Y and subsequent oxidation of metallic Y to Y(III). The detected redox potential of Y(III)/Y approximates to that reported by Han et al.[20] Meanwhile, it can be observed that the redox peaks B_1/B_2 are overlapped with the peaks A_1/A_2, and the reduction peak B_2 is not clearly identified, because the reduction potential of Y(III) is very close to that of Na(I). This phenomenon also was discovered in the electrochemical fabrication of Mg-Nd alloys in our previous work.[21] Thus, it can be deduced that the redox reactions of yttrium on the tungsten electrode is a one-step process because only one pair of redox peaks B_1/B_2 were observed in the cyclic voltammogram after the addition of YCl_3. This is in consistence with the results obtained in previous researches.[20] The redox reactions of Y (III) and Y (0) are represented as follows:

$$Y\,(III) + 3e^- \leftrightarrow Y\,(0) \qquad [1]$$

Fig. 3a shows the cyclic voltammograms of different scan rates measured on a tungsten electrode (d = 1.0 mm) after adding YCl_3 in

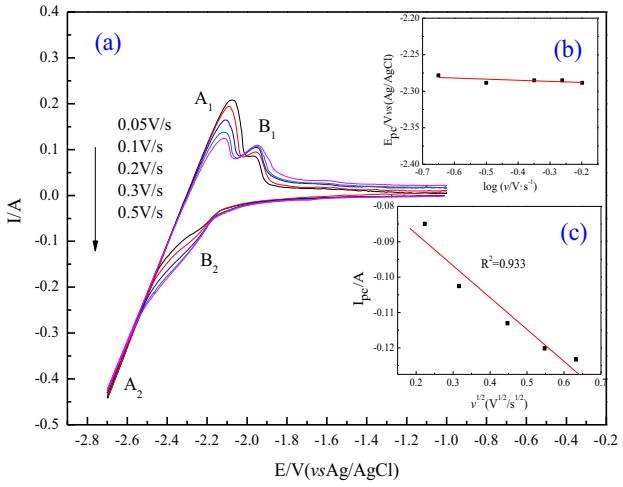

Figure 3. (a) Cyclic voltammograms at different scan rates (0.05∼0.5 V/s) measured on a tungsten electrode (d = 1mm) after addition of 0.6 mol% YCl_3 in a NaCl-KCl system at 973K. (b) The relationship between the cathodic potential and the logarithm of the scan rate. (c) The relationship between cathodic peak current and the square root of the scan rate.

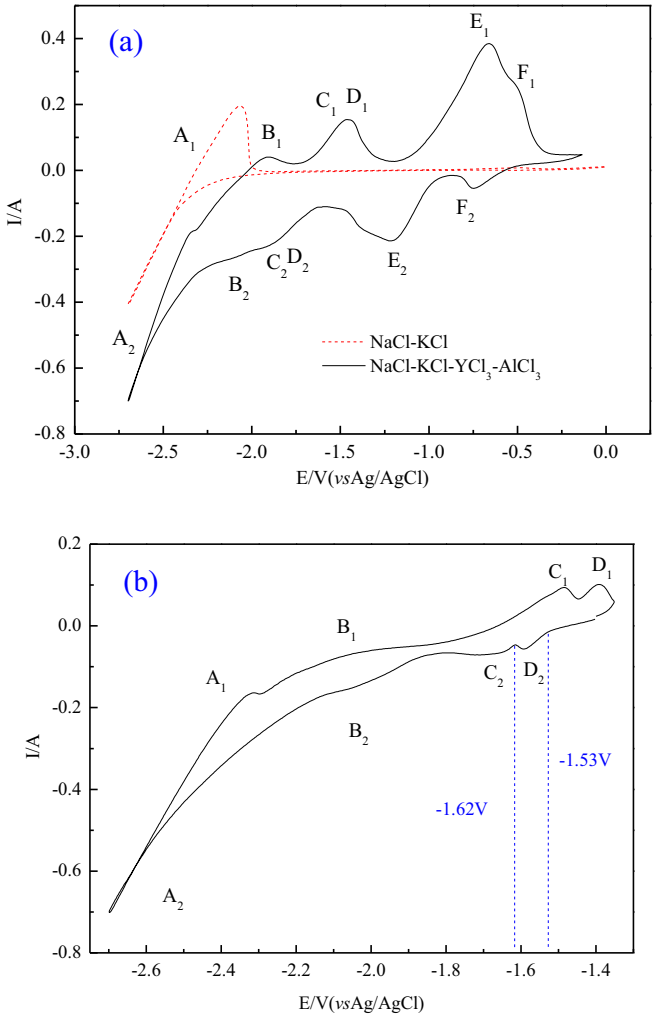

Figure 4. (a) Cyclic voltammograms measured at a tungsten electrode (d = 1 mm) before and after the addition of 1.5 mol% YCl_3 and 1.5 mol% $AlCl_3$ into the NaCl-KCl system at 973K (−2.7∼0V), scan rate = 0.1 V/s. (b) Cyclic voltammogram in the scan range of −2.7∼−1.3 V measured on tungsten electrode.

eutectic NaCl-KCl at 973K. It can be seen that in the scan rate range from 0.05 to 0.5 V/s, the peak potential shifts slightly as the scan rate increases. The peak potential of B_2 presents a linear relationship to the logarithm of the scan rate as shown in Fig. 3b. Therefore, the reduction of Y(III) to metallic Y should be a quasi-reversible process. In addition, the cathodic peak current is approximately linear with the square root of the scan rate (shown in Fig. 3c), indicating that the electrochemical reduction process of Y(III) is controlled by the diffusion step.[22] For soluble-insoluble systems, the diffusion coefficient of Y(III) in molten salts can be calculated by the Berzins-Delahay equation.[23]

$$I_P = -0.61nFSC^0\left(\frac{nF}{RT}\right)^{1/2} D^{1/2}v^{1/2} \quad [2]$$

Where: I_p is the peak current (A); n corresponds to the number of exchanged electrons; F is the Faraday constant (96485C·mol^{-1}); S is the electrode surface area (cm^2); C^0 is the molar concentration (mol/cm^3); R is the molar gas constant [8.314 J/(mol·K)]; T represents the temperature (K); v is the scan rate (V/s), D is the diffusion coefficient (cm^2/s) and calculated to be 2.8 × 10^{-5}cm^2/s.

Y–Al alloy formation mechanism.—$AlCl_3$ was added to the molten NaCl-KCl-YCl_3 salts at 973K and cyclic voltammetry was performed to investigate the formation mechanism of Y-Al alloys. The results are shown in Fig. 4a. It can be seen that several pairs of new oxidation and reduction peaks appear on the cyclic voltammogram curve (solid line) after the addition of $AlCl_3$ compared to the curve of the purified blank salts (dotted line). As mentioned above, A_1/A_2 and B_1/B_2 are attributed to the redox couples of Na(I)/Na and Y(III)/Y, respectively. Peaks E_1/E_2 are associated with the reduction of Al (III) and oxidation of Al.[15] Since a small amount of Al form alloys with the tungsten electrode, there is a pair of insignificant redox peaks F_1/F_2 at the potential more positive than that of peaks E_1/E_2, which correspond to the deposition and dissolution of the Al-W alloy. This phenomenon has also been observed by Su et al. when they prepared Dy-Al alloys by electrodeposition.[13] It can be inferred that the redox peaks C_1/C_2 and D_1/D_2, which have very close potentials, are related to the deposition of Y (III) on pre-deposited Al to form different intermetallic compounds:

$$Y\,(III) + 3e^- + xAl \rightarrow YAl_x \quad [3]$$

The scan range was changed in order to clearly identify the redox couples C_1/C_2 and D_1/D_2 because they are very close to each other. When the positive potential is limited to −1.35 V, the C_1/C_2 and D_1/D_2 peaks can be clearly distinguished in Fig. 4b. According to the Y-Al binary phase diagram,[24] five Y-Al intermetallic compounds can be formed at 973 K. However, only two signals corresponding to Y-Al intermetallic compounds were detected in the cyclic voltammogram curve. It is deduced that the deposition potentials of other Y-Al intermetallic compounds are similar to the signals of C_1/C_2 and D_1/D_2 and these compounds form very slowly, resulting in the non-detectable signals of the other intermetallic compounds.[25,26] Moreover, after $AlCl_3$ was introduced into the molten melts, the anodic peak current corresponding to the dissolution of Y (signal B_1) decreased significantly. Because when $AlCl_3$ is added to the melts, some of the Y forms alloy with Al, and the mass of Y(0) oxidized to Y(III) decreased, which reduces the corresponding anodic current.

Open circuit chronopotentiometry, which can be used to explore the formation of intermetallic compounds and to calculate the Gibbs energies during their formation processes,[27,28] was employed to investigate the electrochemical preparation of Y-Al alloys in the present study. Therefore, potentiostatic electrolysis at −2.5 V (vs Ag/AgCl) was carried out in the NaCl-KCl-YCl_3-$AlCl_3$ melts at 973K for 60 s, and then the open circuit potential of the electrode was recorded versus time. Fig. 5 shows the open circuit chronopotentiometry curve measured on the tungsten electrode in molten NaCl-KCl-YCl_3-$AlCl_3$.

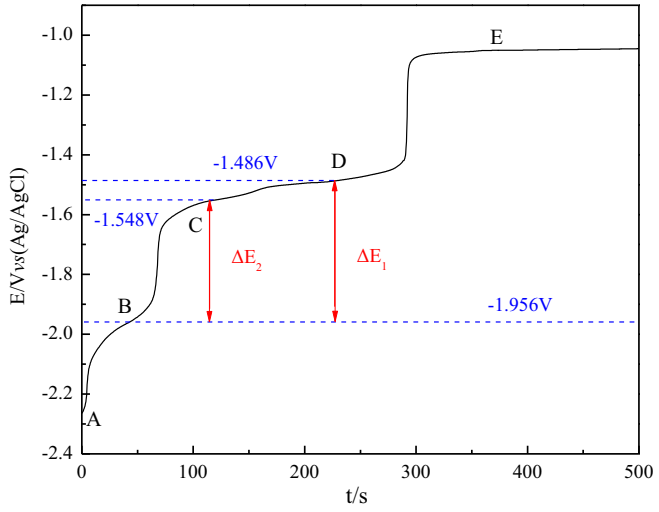

Figure 5. The open circuit chronopotentiometry curve recorded on a tungsten electrode after electrodepositing at −2.5 V vs Ag/AgCl for 60 s in the NaCl-KCl-YCl_3 (1.5 mol%) -$AlCl_3$ (1.5 mol%) melts.

Table I. Thermodynamic properties of Y in the two-phase co-existence states.

Plateau	E/V(vs Ag/AgCl)	ΔE/V(vs Y(III)/Y)	$\Delta\overline{G}_Y$/(KJ/mol)	a_Y
B	-1.956 ± 0.005			
C	-1.548 ± 0.002	0.408 ± 0.007	-118.09 ± 2.03	4.57×10^{-7}
D	-1.486 ± 0.002	0.470 ± 0.007	-136.04 ± 2.03	4.97×10^{-8}

Initially, the potential was maintained at about −2.25 V (platform A), which is attributed to the dissolution of Na metal and corresponds to the Na(I)/Na redox couple. Afterwards, four platforms B, C, D, and E can be observed at −1.96, −1.55, −1.49 and −1.05 V, respectively. The platform B is related to the dissolution of Y(0) to Y(III). The two adjacent platforms C and D can be interpreted as the coexistence of different Y-Al intermetallic compounds. The last platform, E, is ascribed to the oxidation of Al(0) to Al(III).[15] The above results are consistent well with the cyclic voltammetry analysis. According to the Y-Al phase diagram,[24] there are five types of solid intermetallic compounds, including YAl_3, YAl_2, YAl, Y_3Al_2 and Y_2Al, present in the binary system at 973K. The plateau D at −1.55 V is related to the intermetallic compound YAl_3 due to its highest aluminum content among these five Y-Al intermetallic compounds and is therefore first reduced. By analogy, it can be considered that the platform C corresponds to YAl_2. This phenomenon is similar to the preparation of Y-Al alloys in molten LiCl-KCl.[19] Thus, it can be deduced that the possible equilibrium responses for the platforms C and D in Fig. 5 are as follows:

$$\text{D: Y (III)} + 3e^- + 3\text{Al} \rightleftharpoons YAl_3 \quad [4]$$

$$\text{C: } 2YAl_3 + \text{Y (III)} + 3e^- \rightleftharpoons 3YAl_2 \quad [5]$$

The results of the open circuit chronopotentiometry illustrate that the electrochemical co-deposition process of Y-Al alloys includes two consecutive steps. Firstly, Al(III) ions are reduced on the tungsten electrode to form a pure liquid metal film, shaping a metallic Al electrode. Then, Y(III) ions are under-potentially deposited on an Al-plated electrode to form Y-Al alloys. The two consecutive steps equilibrium reactions can be described as follow:

$$x\text{Al (III)} + 3xe^- \rightarrow x\text{Al} \quad [6]$$

$$y\text{Y (III)} + x\text{Al} + 3ye^- \rightarrow \text{Y}_y\text{Al}_x \quad [7]$$

The overall reaction can be expressed as:

$$x\text{Al (III)} + y\text{Y (III)} + 3(x+y)e^- \rightarrow \text{Y}_y\text{Al}_x \quad [8]$$

In fact, the deposition of Y(III) is essentially coincident with the under-potential deposition on the active Al cathode. In virtue of the depolarization effect, the co-deposition of yttrium and aluminum offers more positive potential than pure yttrium on tungsten electrode, as shown in cyclic voltammograms and open circuit chronopotentiometry. It can be expressed from the following equilibrium potential of the Y/Y_yAl_x system referred to Equation 9

$$E_{Y(III)/Y_yAl_x} = E^0_{Y(III)/Y} - \frac{RT}{nF}\ln[a_Y(\text{in}Y_yAl_x)] \quad [9]$$

Where $E^0_{Y(III)/Y}$ designates the equilibrium potential of the pure Y element, $a_Y(\text{in}Y_yAl_x)$ represents the activity of Y in the intermetallic compound Y_yAl_x. The relationship of $E_{Y(III)/YyAlx} > E^0_{Y(III)/Y}$ is obvious since $a_Y(\text{in}Y_yAl_x) < 1$. Additionally, the activity of Y varies in different Y-Al intermetallic compounds, so two potential platforms corresponding to two different Y-Al intermetallic compounds appear in the open-circuit potential transient curve.

The equilibrium potential obtained by electrodeposition of pure Y metal on a tungsten electrode can be converted to an electromotive force for Y(0), which are relevant to activity of Y and the relative partial molar Gibbs energy in two phase co-existence of Y-Al alloys, by the following expression:[29]

$$\Delta\overline{G}_Y = -3F\Delta E = RT\ln a_Y \quad [10]$$

Where a_Y is the activity of yttrium in the Y-Al alloys, choosing pure Y as the standard state; $\Delta\overline{G}_Y$ represents the relative partial molar Gibbs energy of Y in the Y-Al alloys. The calculated thermodynamic properties of Y are listed in Table I. It was found that the activity of Y in the two-phase coexistence state is about 10^{-7} to 10^{-8}. Based on the relative partial molar Gibbs energies, the standard molar Gibbs energies of Y-Al intermetallic compounds can be estimated, and the calculated standard molar Gibbs energies of formation for different Y-Al intermetallic compounds are presented in Table II.

Electrolysis and characterization of Y−Al alloys.—According to the results of the cyclic voltammetry and the open circuit chronopotentiometry, Al(III) ions are preferentially reduced on the inert electrode. In other word, the formation of Al is quite easy than that of Y. Generally, a fairly negative potential[30,31] is selected during the potentiostatic electrolysis to facilitate the deposition of an active metal whose reduction potential is more negative and the alloy formation. Therefore, potentiostatic electrolysis was carried out at −2.2 V (vs Ag/AgCl) on a tungsten electrode at 973K for 10 hours in the eutectic NaCl-KCl melts containing 1.5 mol% YCl_3 and 1.5 mol% $AlCl_3$. Fig. 6 shows the XRD pattern of the alloys obtained by potentiostatic electrolysis. The attained peaks are identified as YAl_2, YAl_3 and YAl phases. It is obvious that the intermetallic compounds of YAl_2 and YAl_3 correspond to platforms C and D occurred on the open circuit chronopotentiometry curve. Besides these two phases, the YAl intermetallic compound was also identified, although the electrochemical signals associated with it were not detected in the cyclic voltammetry and open circuit chronopotentiometry. In effect, Y(III) ions in the melts were reduced to yttrium on preferentially deposited aluminum to form different intermetallic compounds during electrolysis. As mentioned above, the intermetallic compound with higher content of Al would be easily produced. In other words, the Y-rich phase of YAl formed in the later period of electrolysis. This is entirely true in the present experiments. In the initial stage of electrolysis, the molar

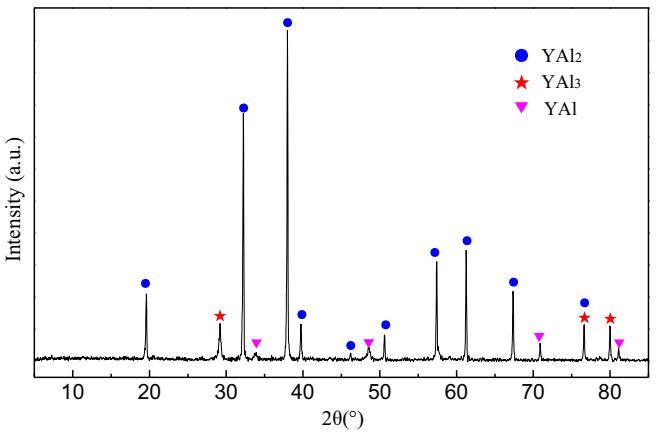

Figure 6. XRD pattern of cathodic products obtained in molten NaCl-KCl-YCl_3-$AlCl_3$ salts at −2.2 V (vs Ag/AgCl) by potentiostatic electrolysis for 10 h.

Table II. Standard molar Gibbs energies of formation for Y-Al intermetallic compounds.

Intermetallic compounds	Equation	$\Delta\overline{G}_Y$/(KJ/mol)
YAl_3	$\Delta G^{\theta}_f(YAl_3) = -3F\Delta E_1$	-136.04 ± 2.03
YAl_2	$\Delta G^{\theta}_f(YAl_2) = 1/3[2\Delta G^{\theta}_f(YAl_3) - 3F\Delta E_2]$	-130.06 ± 2.03

concentration of $AlCl_3$ in the melts is nearly equal to that of YCl_3, and only two Al-rich phases of YAl_2 and YAl_3 intermetallic compounds generate via coreductiuon, but the intermetallic compound YAl which is Y-rich phase, has not formed. Therefore, the electrochemical signals corresponding to YAl did not appear in the cyclic voltammetry and open circuit chronopotentiometry. After electrolysis lasts for a long time, the content of Al(III) ions in molten salts decreases much faster than that of Y(III) ions along with the formation of YAl_2 and YAl_3. On the other hand, $AlCl_3$ is more prone to volatilize than YCl_3 at the experimental temperature. Consequently, the concentration of $AlCl_3$ became much lower than that of YCl_3, and thus the deposition potential is negative enough to generate a Y-rich phase intermetallic compound YAl. However, it should be noticed that $AlCl_3$ in the melts has not been completely depleted even in the late period of electrolysis, and the generated Y(0) could still alloy with Al to form a Y-rich phase intermetallic compound. In consequence, pure Y metal cannot be generated in the cathodic alloys.

In order to further investigate the distribution of Y and Al elements in Y-Al alloys gained in the experiment, the microstructure and chemical composition of the alloys were determined by SEM and EDS. Fig. 7 shows the SEM image of Y-Al alloys obtained by constant potential electrolysis at 973 K. It can be seen that the alloys are in the round and granular shape. Combining with the previous electrochemical measurements, it can be inferred that the Al(III) ions will first be reduced on the tungsten electrode in liquid state at the electrolytic temperature of 973 K. Subsequently, the under-potential deposition of Y(III) ions takes place in liquid Al to produce solid particles of the intermetallic compound, which are detached from the Al electrode and dropped to the bottom of the crucible. At the end of the experiment, we collected the product from the bottom of the crucible and only a small amount of salts attached to the cathode, which also verified this conjecture. EDS analysis of the different regions in Fig 7 marked A and B indicates that the sediments are merely composed of Y and Al. Both in points A and B, the atomic ratio of Al:Y is roughly 2. Considering the measurement error, it can be speculated that the alloys are mainly composed of YAl_2, as well as a small amount of YAl_3 and YAl. In general, the EDS results of Y-Al alloys are in good accordance with those from XRD analysis.

Conclusions

The electrochemical behavior of yttrium in NaCl-KCl eutectic at 973 K on a tungsten electrode was investigated by cyclic voltammetry. The results show that the reduction of Y(III) to metallic Y is a single-step process with three electrons exchanged in the eutectic NaCl-KCl melts at about −2.1 V (vs Ag/AgCl). In the NaCl-KCl system, the deposition/dissolution reaction of yttrium is considered to be a quasi-reversible and diffusion-controlled process. The diffusion coefficient of Y(III) ions is estimated to be 2.8×10^{-5} cm^2/s.

Cyclic voltammetry obtained in molten NaCl-KCl-YCl_3-$AlCl_3$ presents two pairs of redox peaks for Y-Al intermetallic compounds. According to the open circuit chronopotentiometry analysis, it can be deduced that the presence of the two platforms at −1.55 and −1.49 V are attributed to the equilibrium reactions of YAl_2 and YAl_3, respectively. The reduction of Y(III) in the NaCl-KCl-YCl_3-$AlCl_3$ melts is likely an under-potential deposition process. From the electromotive force measurements, the thermodynamic properties, such as the activity of Y in different Y-Al intermetallic compounds, relative partial molar Gibbs energies of Y, as well as the formation Gibbs energies of YAl_2 and YAl_3 could be evaluated.

The Y-Al alloys were obtained by potentiostatic electrolysis at −2.2 V in the molten NaCl-KCl-YCl_3-$AlCl_3$ for 10 h. During the electrolysis process, Al(III) was considered to be preferentially reduced to Al metal, and then under-potential deposition of Y (III) took place on the pre-reduced aluminum to form Y-Al alloys. The obtained alloys are in the round and granular shape, and mainly composed of YAl_2, as well as a small amount of YAl_3 and YAl phases. The Y-rich phase intermetallic compound YAl just generated at the later period of electrolysis when the concentration of $AlCl_3$ in the melts is fairly low.

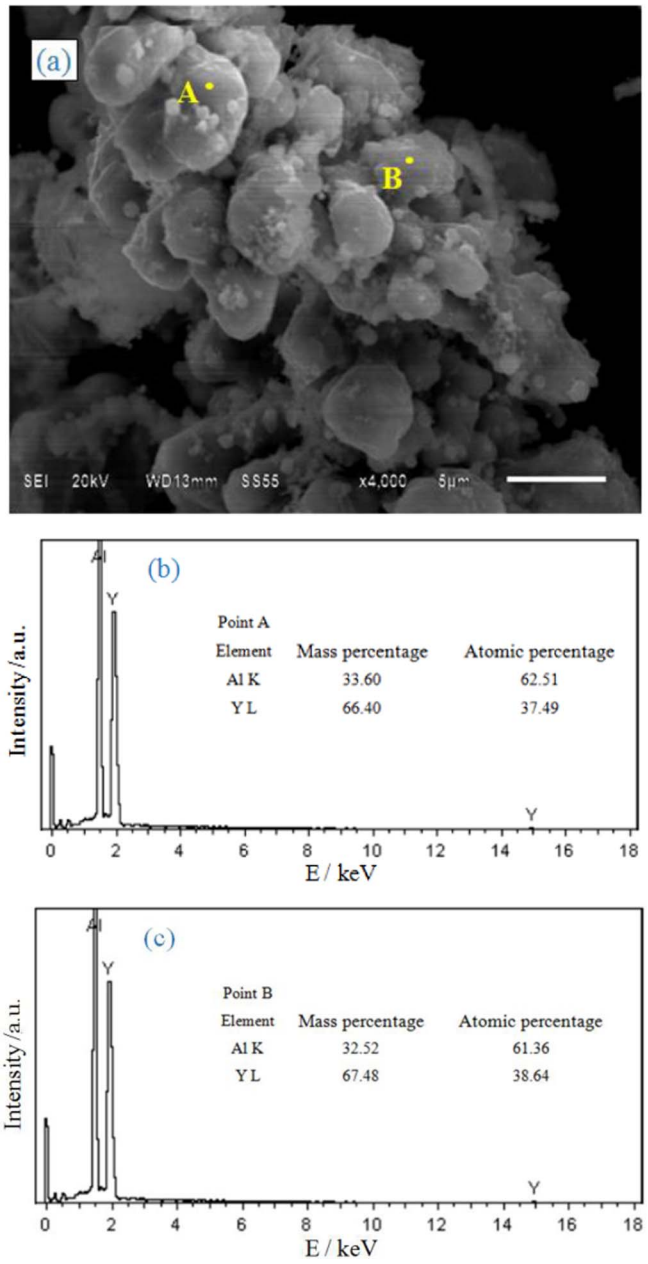

Figure 7. SEM image (a) and EDS analysis of the points labeled A, B of the Y-Al alloy (b, c) by electrolysis at 973 K from NaCl-KCl-YCl_3 (1.5 mol%)-$AlCl_3$ (1.5 mol%) melt.

These investigations demonstrate that it is feasible to prepare Y-Al alloys by the electrochemical coreduction of Y (III) and Al (III) in molten NaCl-KCl-YCl_3-$AlCl_3$.

Acknowledgments

This work was financially supported by the National Natural Science Foundation of China (51204002 and 51574003), the Developing Program Foundation for the Excellent Youth Talents of Higher Education of Anhui Province (gxyq2018012) and the Foundation of Anhui Province Key Laboratory of Metallurgical Engineering & Resources Recycling (KF17-04).

ORCID

Jiwen He https://orcid.org/0000-0001-5751-6698
Zhongsheng Hua https://orcid.org/0000-0002-5984-1336

References

1. K. Binnemans, P. T. Jones, B. Blanpain, T. V. Gerven, Y. Yang, A. Walton, and M. Buchert, *J. Clean. Prod.*, **51**, 1 (2013).
2. K. Przybylski, A. J. Garratt-Reed, and G. J. Yurek, *J. Electrochem. Soc.*, **135**, 509 (1988).
3. X. Sun, M. Nour, Y. Wang, and D. Li, *Wear*, **302**, 1624 (2013).
4. J. Zhao, J. Zhang, W. Liu, G. Wu, and L. Zhang, *Mat. Sci. Eng. A - Struct.*, **650**, 240 (2016).
5. N. Das and D. Das, *J. Rare Earth.*, **31**, 933 (2013).
6. S. A. Shakhshir and M. Medraj, *J. Phase Equilib. Diff.*, **27**, 231 (2006).
7. R. Raggio, G. Borzone, and R. Ferro, *Intermetallics*, **8**, 247 (2000).
8. M. Khrussanova, J. L. Bobet, M. Terzieva, B. Chevalier, D. Radev, P. Peshev, and B. Darriet, *J. Alloy. Compd.*, **307**, 283 (2000).
9. V. S. Timofeev, A. A. Turchanin, A. A. Zubkov, and I. A. Tomilin, *Thermochim. Acta*, **299**, 37 (1997).
10. Y. Chen, Q. Xu, Q. Song, H. Li, R. Djouani, and X. Lu, *J. Electrochem. Soc.*, **164**, 380 (2017).
11. H. Konishi, T. Nohira, and Y. Ito, *Thermochim. Acta*, **48**, 563 (2003).
12. Y. Castrillejo, M. R. Bermejo, A. I. Barrado, and A. M. Martínez, *Thermochim. Acta*, **50**, 2047 (2005).
13. L. Su, K. Liu, Y. Liu, L. Wang, L. Yuan, L. Wang, Z. Li, X. Zhao, Z. Chai, and W. Shi, *Thermochim. Acta*, **147**, 87 (2014).
14. M. R. Bermejo, E. Barrado, A. M. Martínez, and Y. Castrillejo, *J. Electroanal. Chem.*, **617**, 85 (2008).
15. Y. Yan, H. Tang, M. Zhang, Y. Xue, W. Han, D. Cao, and Z. Zhang, *Thermochim. Acta*, **59**, 531(2012).
16. X. Li, Y. Yan, M. Zhang, Y. Xue, W. Han, H. Tang, D. Ji, and Z. Zhang, *J. Electrochem. Soc.*, **161**, 48 (2014).
17. M. Li, Y. Liu, W. Han, S. Wang, M. Zhang, and Y. Yan, *Metall. Mater. Trans. B*, **46**, 644 (2015).
18. Y. Li, F. Wang, M. Zhang, W. Han, and Y. Tian, *J. Rare Earth.*, **29**, 378 (2011).
19. Y. Yan, X. Yang, Y. Huang, Y. Xue, M. Zhang, W. Han, and Z. Zhang, *Rare Metal Mat. Eng.*, **45**, 272 (2016).
20. W. Han, Q. Zhao, J. Wang, J. Wang, M. Li, W. Liu, M. Zhang, X. Yang, and Y. Sun, *J. Rare Earth.*, **35**, 90 (2017).
21. Z. Hua, H. Liu, J. Wang, J. He, S. Xiao, Y. Xiao, and Y. Yang, *ACS Sustain. Chem. Eng.*, **5**, 8089 (2017).
22. M. Li, B. Liu, N. Ji, Y. Sun, W. Han, T. Jiang, S. Peng, Y. Yan, and M. Zhang, *Thermochim. Acta*, **193**, 54 (2016).
23. T. Store and G. M. Haarbergand R. Tunold, *J. Appl. Electrochem.*, **30**, 1351 (2000).
24. *Binary Alloy Phase Diagrams*, second ed. ASM International, 1996.
25. X. Li, Y. Yan, M. Zhang, H. Tang, D. Ji, and W. Han, *Thermochim. Acta*, **135**, 327 (2014).
26. T. Iida, T. Nohira, and Y. Ito, *Thermochim. Acta*, **48**, 901 (2003).
27. Y. Castrillejo, P. Fernández, J. Medina, P. Hernández, and E. Barrado, *Thermochim. Acta*, **56**, 8638 (2011).
28. Y. Castrillejo, M. R. Bermejo, E. Barrado, and A. M. Martínez, *Thermochim. Acta*, **51**, 1941 (2006).
29. W. Han, N. Ji, J. Wang, M. Li, X. Yang, Y. Sun, and M. Zhang, *Rsc Adv.*, **7**, 31682 (2017).
30. H. Tang, Y. Yan, M. Zhang, X. Li, Y. Huang, Y. Xu, X. Yun, H. Wei, and Z. Zhang, *Thermochim. Acta*, **88**, 457 (2013).
31. S. Kobayashi, K. Kobayashi, T. Nohira, R. Hagiwara, T. Oishi, and H. Konishi, *J. Electrochem. Soc.*, **158**, 142 (2011).